Analyst

PAPER

View Article Online
View Journal | View Issue

Cite this: *Analyst*, 2015, **140**, 7434

A FRET-based ratiometric fluorescent aptasensor for rapid and onsite visual detection of ochratoxin A†

Jing Qian,[a] Kan Wang,[a] Chengquan Wang,[b] Mengjuan Hua,[a] Zhenting Yang,[a] Qian Liu,[a] Hanping Mao[a] and Kun Wang*[a]

Received 12th July 2015,
Accepted 28th August 2015

DOI: 10.1039/c5an01403d

www.rsc.org/analyst

A color change observable by the naked eye to indicate the content of an analyte is considered to be the most conceivable way of various sensing protocols. By taking advantage of the Förster resonance energy transfer (FRET) principles, we herein designed a dual-emission ratiometric fluorescent aptasensor for ochratoxin A (OTA) detection *via* a dual mode of fluorescent sensing and onsite visual screening. Amino group-modified OTA's aptamer was firstly labeled with the green-emitting CdTe quantum dots (gQDs) donor. The red-emitting CdTe QDs (rQDs) which were wrapped in the silica sphere could serve as the reference signal, while the gold nanoparticle (AuNP) acceptors were attached on the silica surface to bind with the thiolated complementary DNA (cDNA). The hybridization reaction between the aptamer and the cDNA brought gQD–AuNP pair close enough, thereby making the FRET occur in the aptasensor fabrication, while the subsequent fluorescence recovery induced by OTA was obtained in the detection procedure. Based on the red background of the wrapped rQDs, the aptasensor in response to increasing OTA displayed a distinguishable color change from red to yellow-green, which could be conveniently readout in solution even by the naked eye. Since the bioconjugations used as the aptasensor can be produced at large scale, this method can be used for *in situ*, rapid, or high-throughput OTA detection after only an incubation step in a homogeneous mode. We believe that this novel aptasensing strategy provides not only a promising method for OTA detection but also a universal model for detecting diverse targets by changing the corresponding aptamer.

Introduction

The Food and Agriculture Organization estimated that about 25% of the world's food crops are contaminated by mycotoxins per year.[1] Ochratoxin A (OTA), one of the most toxic and widespread naturally occurring mycotoxins, exists in a variety of food products *i.e.* cereals, wheat, corn, oats, coffee beans, beer, coffee, grape juice, and wine.[2] OTA has nephrotoxic, immunotoxic, hepatotoxic, teratogenic, and carcinogenic effects and has been considered to be a potential carcinogen (group 2B) for humans.[2,3] Even worse, OTA is chemically stable and consequently may resist cooking treatments at quite high temperatures. Of major concern for human health, it is urgent to develop a sensitive, cheap, rapid, and simple method to detect OTA for food safety and quality control purposes.[4] The currently accepted testing methods, such as high performance liquid chromatography,[5] mass spectrometry,[6] and gas chromatography[7] are quite sensitive. However, some disadvantages such as complex and time-consuming sample preparation procedures, sophisticated equipment, and trained personnel limit their practical use.[8] As an alternative, enzyme-linked immunosorbent assays (ELISA) based on antigen–antibody interactions have also been developed for OTA detection.[9–11] These assays have obvious merits *i.e.* simplicity and reliability; however, it needs stable detection conditions and expensive antibodies.[12,13]

Aptamers are SELEX (systematic evolution of ligands by exponential enrichment)-produced short synthetic single-stranded oligonucleotides, which possess strong binding affinity to target molecules. As a novel recognition element, aptamers are attractive alternatives to antibodies due to the advantages of better thermal stability, accessibility, feasible chemical synthesis and easy modifications with functionalities such as thiol and amino groups.[14,15] Ever since the discovery of the aptamer specific for OTA in 2008,[16] different versions of aptasensors have come out towards OTA determination, combining with a variety of signal transducers including fluorescence,[17,18] electrochemistry,[19,20] electrochemiluminescence,[21] and colorimetry.[22] Among them, the fluorescence-based

[a]*Key Laboratory of Modern Agriculture Equipment and Technology, School of Chemistry and Chemical Engineering, Jiangsu University, Zhenjiang 212013, P. R. China. E-mail: wangkun@ujs.edu.cn; Fax: +86 511 88791708; Tel: +86 511 88791800*

[b]*Changzhou College of Information Technology, Changzhou 213164, P. R. China*

†Electronic supplementary information (ESI) available. See DOI: 10.1039/c5an01403d

method has attracted great attention owing to its sensitivity and flexibility. Some of these reported fluorescent aptasensors for OTA are based on the quenching of fluorescence signals,[17] while other research studies have been focused on the enhancement of fluorescence.[18,23] Very recently, a multifunctional aptasensor has been developed by our group for rapid detection of OTA; its sensitivity can be effectively improved by using a heavy CdTe quantum dot (QD) label loaded in and on a SiO_2 nanocarrier.[24] To the best of our knowledge, all of the reported fluorescent aptasensors for OTA are based on the change in fluorescence intensity of a single-emissive lumophore. Variations in these aptasensors such as probe concentration, instrumental efficiency, and environmental conditions cannot ensure a precise determination.[25]

The ratiometric fluorescence technique provides built-in correction for environmental interference and eliminates the fluctuation of excitation light intensity by measuring the changes of emission intensity ratios at two different wavelengths, and therefore possesses advantages of improved sensitivity and accuracy.[26,27] Compared with the single-emissive fluorescence assay, the signal variation of the ratiometric fluorescence assay is easier to be distinguished by the naked eye.[27] As we all know, a color change observable by the naked eye to indicate the content of an analyte, is considered to be the most conceivable way of various sensing protocols. In this sense, there is an increasing desire to develop such simple, onsite, cost-effective methodology towards OTA detection for field use. Förster resonance energy transfer (FRET) is a powerful technique to investigate various molecular interactions and changes in the molecular structure.[28–30] It is reported that in a FRET process, separate donors and acceptors are brought in close proximity through antigen/antibody interactions.[31] Compared with traditional methods, FRET-based assays are more advantageous with fast liquid-phase binding kinetics, long-term stability, and homogeneous detection.[32] However, typical organic dyes used as donors or acceptors always suffer from several limitations, such as low stability, photobleaching, and short observation time, which seriously deteriorate the performance of the sensors.[33] In recent years, semiconductor QD-donor and gold nanoparticle (AuNP)-acceptor pair has been reported to assemble specific immunosensors for a series of targets such as carcinoembryonic antigen,[34] *Staphylococcus aureus*,[35] and glutathione.[36]

By taking advantage of the FRET principles, for the first time we have developed a dual-emission ratiometric fluorescent aptasensor for rapid and high-throughput detection of OTA *via* a dual mode of fluorescent sensing and onsite visual screening. Amino group-modified aptamers specific for OTA were firstly labeled with the green-emitting CdTe QDs (gQDs) donor. The red-emitting CdTe QDs (rQDs) which were wrapped in the silica sphere could serve as the reference signal, while the AuNPs attached on the silica surface were used as the acceptor to bind with the thiolated complementary DNA (cDNA). The hybridization reaction between the aptamer and cDNA brought gQD–AuNP pair close enough, thereby making the FRET occur and thus result in the fluorescence quenching of gQDs. The presence of OTA in the sensing system would trigger aptamer–OTA complex formation, resulting in the partial release of gQDs into bulk solution. With the background of the wrapped rQDs, the fluorescence variations in response to OTA concentration exhibited continuous changes, which could be conveniently readout in solution even by the naked eye.

Experimental

Reagents

Tetraethylorthosilicate (TEOS), poly(diallyldimethylammonium chloride) (PDDA, 20%, M_W = 200 000–350 000), 3-aminopropyltriethoxysilane (APTS), 3-mercaptopropionic acid (MPA), 1-ethyl-3-(3-dimethylaminopropyl) carbodiimide hydrochloride (EDC), *N*-hydroxysuccinimide (NHS), tris(2-chloroethyl) phosphate (TCEP), OTA, ochratoxin B (OTB), fumonisin B1 (FB1), and aflatoxin B1 (AFB1) standard substances were purchased from Sigma-Aldrich. cDNA: 5′-TGT CCG ATG CTC CCT TTA CGC CAC CCA CAC CCG ATC-SH-3′, aptamer: 5′-NH_2-GAT CGG GTG TGG GTG GCG TAA AGG GAG CAT CGG ACA-3′, and aptamer*: 5′-GAT CGG GTG TGG GTG GCG TAA AGG GAG CAT CGG ACA-NH_2-3′ were purchased from Sangon Biotech Co., Ltd (Shanghai, China). CdTe QDs and AuNPs were prepared according to Zhang's[37] and Qian's[34] methods (ESI†). Double-distilled water was used throughout the study.

Apparatus

Transmission electron microscopy (TEM) images were taken with a JEOL 2100 TEM (JEOL, Japan). Fluorescence (FL) intensity and the corresponding spectra were recorded on a Hitachi F-4500 Fluorescence spectrophotometer (Tokyo, Japan). UV-vis absorption spectra were recorded on a UV-2450 spectrophotometer (Shimadzu, Japan). Zeta potential was received using a Malvern Zetasizer Nano ZS instrument (UK). X-ray photoelectron spectroscopy (XPS) was performed on ESCALAB 250 multitechnique surface analysis system (Thermo Electron Co., USA). All the photographs were taken by a home-used Canon digital camera (IXUS 230 HS, China) under a 365 nm UV lamp in a dark box.

Conjugation of cDNA to rQDs@SiO_2@AuNPs hybrid spheres

The synthesis procedure of rQDs@SiO_2@AuNPs hybrid spheres has been described in the ESI.† The conjugation of cDNA on the surface of rQDs@SiO_2@AuNPs (rQDs@SiO_2@AuNPs–cDNA) was performed according to the reported literature.[38,39] To activate the thiolated cDNA, 40 μL of 100 μM cDNA was added to 10 μL of Tris-HCl buffer (pH = 7.4, 10 mM) containing 100 mM TCEP, and incubated at room temperature for 1 h. Subsequently, the excess TCEP was removed using Millipore's Amicon Ultra-0.5 centrifugal filter device. Then, 3 mL of the as-prepared rQDs@SiO_2@AuNPs suspension was added to the freshly deprotected and purified cDNA solution. The mixture was sonicated for 10 s and incubated under shaking at room temperature for 30 min. With increments of 0.05 M NaCl every 20 min, followed by vortexing and sonication for 10 s, the

concentration of NaCl was finally reached 0.4 M using 2 M NaCl and the mixture was incubated overnight at room temperature. To remove the unbound cDNA, the as-obtained rQDs@SiO_2@AuNPs–cDNA was centrifuged and rinsed thrice, and then redispersed in 3 mL Tris-HCl buffer solution (pH 7.4, 10 mM) containing 120 mM NaCl, 20 mM $CaCl_2$, and 5 mM KCl.

Preparation of the aptamer-coupled gQDs

In a typical synthesis, 1 mL of MPA-capped gQDs was mixed with 40 μL of EDC (1 mM) and 40 μL of NHS (1 mM) and gently stirred for 2 h at room temperature. To immobilize the amino-modified aptamer, 40 μL of 100 μM aptamer was added to the above mixture, followed by gentle shaking overnight. After centrifugation, the as-obtained aptamer-coupled gQDs (aptamer–gQDs) were redispersed into 1 mL of Tris-HCl buffer solution (pH 7.4, 10 mM) containing 120 mM NaCl, 20 mM $CaCl_2$, and 5 mM KCl. For comparison, aptamer*–gQDs were also obtained following the same process except for the use of aptamer* (ESI†).

Fabrication of the ratiometric fluorescent aptasensor

The mixture of the resulting aptamer–gQDs and rQDs@SiO_2@AuNPs–cDNA was continuously shaken for 2 h at 37 °C with the help of a reciprocating oscillator. After centrifugation and washing, the rQDs@SiO_2@AuNPs–cDNA/aptamer–gQDs bioconjugations were redispersed in 4 mL Tris-HCl buffer (pH 7.4, 10 mM) containing 120 mM NaCl, 20 mM $CaCl_2$, and 5 mM KCl and used as the ratiometric fluorescent aptasensor in a further study.

Detection procedures

50 μL of the rQDs@SiO_2@AuNPs–cDNA/aptamer–gQDs bioconjugations and 50 μL of OTA containing solution with various concentrations were mixed and incubated for 60 min at room temperature under gentle shaking. To perform the visual fluorescence detection, the mixture was diluted to a final volume of 250 μL with Tris-HCl buffer (pH 7.4, 10 mM) and transferred to a series of miniwells. The photographs were obtained using the home-used digital camera under UV illumination (λ_{ex} = 365 nm). To perform the spectrometric analysis, the mixed solution was diluted to a final volume of 2 mL with Tris-HCl buffer (pH 7.4, 10 mM) and transferred to the cuvette; its fluorescence spectrum was then recorded accordingly using λ_{ex} = 365 nm.

Results and discussion

Characterization of the rQDs@SiO_2@AuNPs core–satellite hybrid spheres

The as-prepared rQDs had a maximum absorption peak at 587 nm (Fig. S1†) and its size can be calculated to be 3.3 nm using the empirical expression.[40] The resulting aqueous dispersed rQDs@SiO_2 nanospheres (curve b in Fig. 1A) displayed an obvious emission peak centered at ~635 nm, consistent with that of the mother rQDs (curve a in Fig. 1A). The photographs under 365 nm UV illumination showed that both of them emitted red fluorescence (inset in Fig. 1A). The as-prepared rQDs@SiO_2 nanospheres, with an average diameter of 105 nm, had a chemically clean and homogenized structure (Fig. 1B). The presence of the outer silica shell can prevent the direct contact of the rQDs with external solvents and analytes, which made the optical properties of the inner rQDs more stable, thus providing a reliable reference signal for the ratiometric fluorescent aptasensing. Besides, the silica shell can also offer an ideal anchorage substrate for the subsequent AuNPs binding to produce core–satellite hybrid spheres.

AuNPs have become one of the most attractive coating materials due to the strong adsorptive capacity and excellent biocompatibility.[41,42] With a high extinction coefficient and broad absorption spectrum in visible light that overlapped with the emission spectra of usual energy donors, AuNPs played an important role in FRET-based sensors.[33,43] Therefore, the AuNPs with an average diameter of 5 nm estimated by TEM image (Fig. S2†) were obtained by using the $NaBH_4$-mediated reduction of $AuCl_4^-$. The characteristic surface plasmon resonance band located at 513 nm in the UV-vis absorption spectrum (curve a in Fig. 1C) confirmed the successful formation of the well-dispersed and spherical AuNPs in aqueous solution.

The assembly of oppositely charged polyelectrolytes on nanospheres' surface has been widely used as an effective route to fabricate core–satellite hybrid materials.[44,45] In this work, the zeta potential of rQDs@SiO_2 nanospheres at neutral pH was measured to be −23.7 mV, indicating that the silica shell was negatively charged due to the surface hydroxyl groups.[46] The adsorption of a layer of positively charged PDDA on rQDs@SiO_2 switched the zeta potential to a positive value of 35.9 mV. After the subsequent adsorption of negatively charged AuNPs onto the rQDs@SiO_2 surface by means of electrostatic interactions, the zeta potential of the resulting rQDs@SiO_2@AuNPs was 9.3 mV, which demonstrated that AuNPs had been anchored on rQDs@SiO_2 effectively. TEM image (Fig. 1D) displayed that the as-obtained rQDs@SiO_2@AuNPs comprised numerous individual dark nanodots around the silica shells with a crude surface. The XPS spectra of the rQDs@SiO_2@AuNPs hybrid spheres clearly indicated that they were composed of Cd, Te, Si, O, C, N, and Au elements, in accordance with the original constituent elements of CdTe QDs, SiO_2, PDDA, and AuNPs (Fig. 1E). These results indicated that the AuNPs had been adsorbed on the silica shells quite uniformly. The outer silica shell also provided the separation distance which could avoid the potential FRET between the reference rQDs and AuNPs.

Conjugation of cDNA to rQDs@SiO_2@AuNPs hybrid spheres

Thiolated cDNA was conjugated on the rQDs@SiO_2@AuNPs surface through the famous Au–S linkage. High-resolution XPS spectrum of P 2p was ascertained to confirm whether the thiolated cDNA was successfully conjugated to the surface of the rQDs@SiO_2@AuNPs hybrid spheres (Fig. 2A). No clear characterized P 2p peak was observed in the scanning region for rQDs@SiO_2@AuNPs without cDNA coupling (curve a).

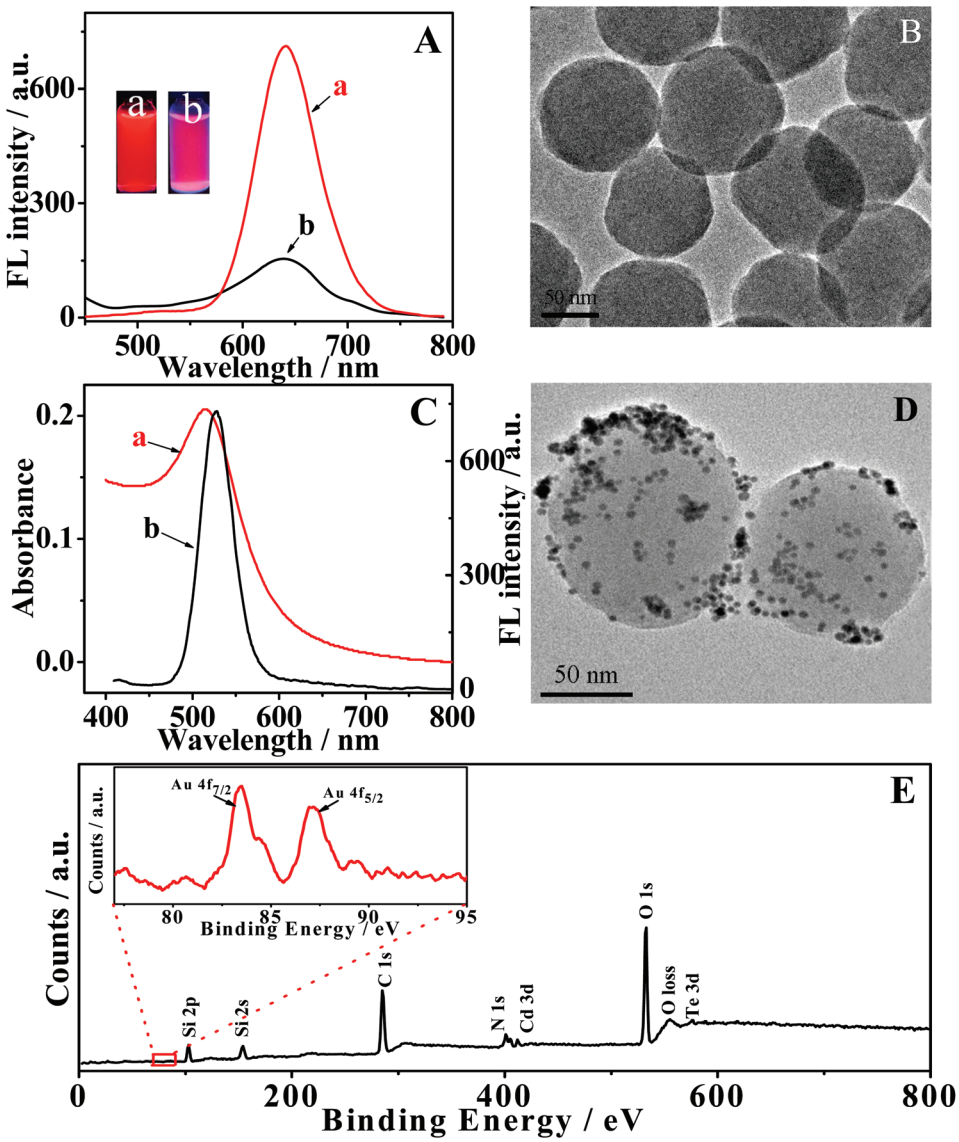

Fig. 1 (A) Fluorescence spectra and the corresponding photographs (inset) of rQDs (a) and rQDs@SiO_2 (b) under UV illumination (λ_{ex} = 365 nm). (B) TEM image of rQDs@SiO_2. (C) UV-vis spectra of AuNPs (a) and the fluorescence spectrum of gQDs (b). (D) TEM image of rQDs@SiO_2@AuNPs hybrid spheres. (E) The wide scan XPS spectrum of rQDs@SiO_2@AuNPs hybrid spheres. Inset: narrow-scan XPS of the Au 4f regions.

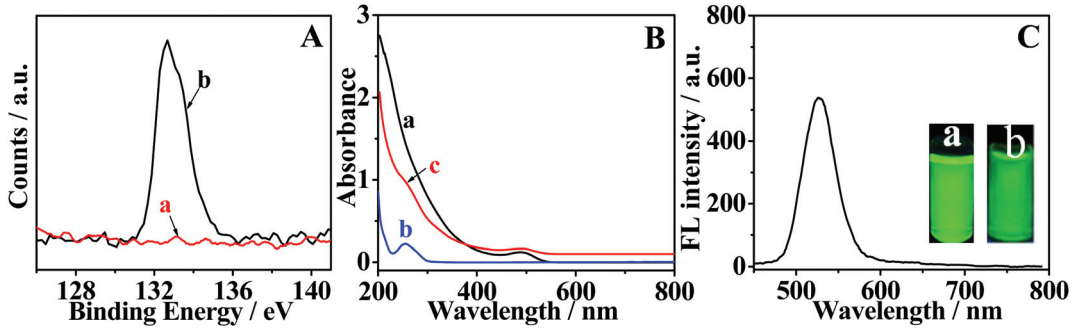

Fig. 2 (A) The high-resolution XPS spectra of P 2p of the resulting rQDs@SiO_2@AuNPs before (a) and after (b) cDNA coupling. (B) UV-vis spectra of gQDs (a), free aptamer (b) and aptamer–gQDs (c). (C) Fluorescence spectrum of aptamer–gQDs. Inset: the photographs of gQDs (a) and aptamer–gQDs (b) under UV illumination (λ_{ex} = 365 nm).

However, the P 2p peak at 132.6 eV was obviously observed in the same region after cDNA coupling (curve b), coming from the phosphate backbone in the cDNA.[47] These results indicated the successful conjugation of cDNA onto the rQDs@SiO_2@AuNPs surface.

Characterization of the aptamer-coupled gQDs

The as-prepared gQDs had a maximum absorption peak at 490 nm (curve a in Fig. 2B) and an emission peak at 530 nm (curve b in Fig. 1C). An appreciable spectral overlap between donor emission and acceptor absorption is essential for a FRET system.[32,34] The result exhibited a large degree of overlap with the emission spectra of gQDs (donor) and the absorption spectra of AuNPs (acceptor) (Fig. 1C). The coupling of amino-modified aptamer on the surface of gQDs was achieved through the amide bond between the carboxylic groups on the MPA-capped gQDs and the amino group in the aptamer by using EDC/NHS chemistry. The aptamer–gQDs conjugations (curve c in Fig. 2B) produced two characteristic absorption peaks: one located at 260 nm for the specific absorbance of the aptamer (curve b in Fig. 2B) and the other located at 493 nm for the absorption of the gQD itself with 3 nm red-shifts. In comparison with the original gQDs (curve b in Fig. 1C), the resulting aptamer–gQDs conjugations (Fig. 2C) showed a reduced fluorescence intensity at 530 nm, probably due to the biomolecular fluorescence quenching effect.[48] However, both gQDs and aptamer–gQDs emitted strong green fluorescence under 365 nm UV illumination (inset in Fig. 2C).

Fabrication of the aptasensor

Except for a good spectral overlap between donor emission and acceptor absorption, another key factor that influences the FRET process is the distance between the donor and acceptor within the range of 2–9 nm.[33] In our proposal, gQDs were selected as a donor to label the aptamer and AuNPs attached on the rQDs@SiO_2 were used as an acceptor to immobilize cDNA. The main strategy to fabricate the ratiometric fluorescent aptasensor is to use the highly specific DNA hybridization event to bring the donor (gQDs) and acceptor (AuNPs) in close proximity for efficient FRET, with the fully wrapped rQDs as a reference signal (step 1 in Fig. 3A). The energy transfer process from gQD donor to AuNP acceptor was observed by the emission changes of rQDs@SiO_2@AuNPs–cDNA/aptamer–gQDs bioconjugations at 530 nm contributed by gQDs. As indicated, the emission of gQDs at 530 nm was almost completely quenched, whereas the emission at 635 nm contributed by the wrapped rQDs remained constant (curve a in Fig. 3B). Control experiments showed that there was increasing emission of gQDs when the increasing aptamer*–gQDs were conjugated with rQDs@SiO_2@AuNPs–cDNA (Fig. S3†). Taking 3 pairs of nucleotides accounting for 1.0 nm and the rigid-rod structure of the DNA duplex into consideration,[49] the energy transfer cannot effectively occur when the donor-to-acceptor distance was increased to 12.0 nm (Scheme S1†). The weak fluorescence intensity at 530 nm of the rQDs@SiO_2@AuNPs–cDNA/aptamer–gQDs bioconjugations could be attributable to FRET between the gQDs and AuNPs.

Working principle for the ratiometric fluorescent detection of OTA

Due to the high affinity and selectivity between the specific aptamer and its target, the rQDs@SiO_2@AuNPs–cDNA/aptamer–gQDs bioconjugations were used as the ratiometric fluorescent aptasensor for the rapid and homogeneous detection of OTA

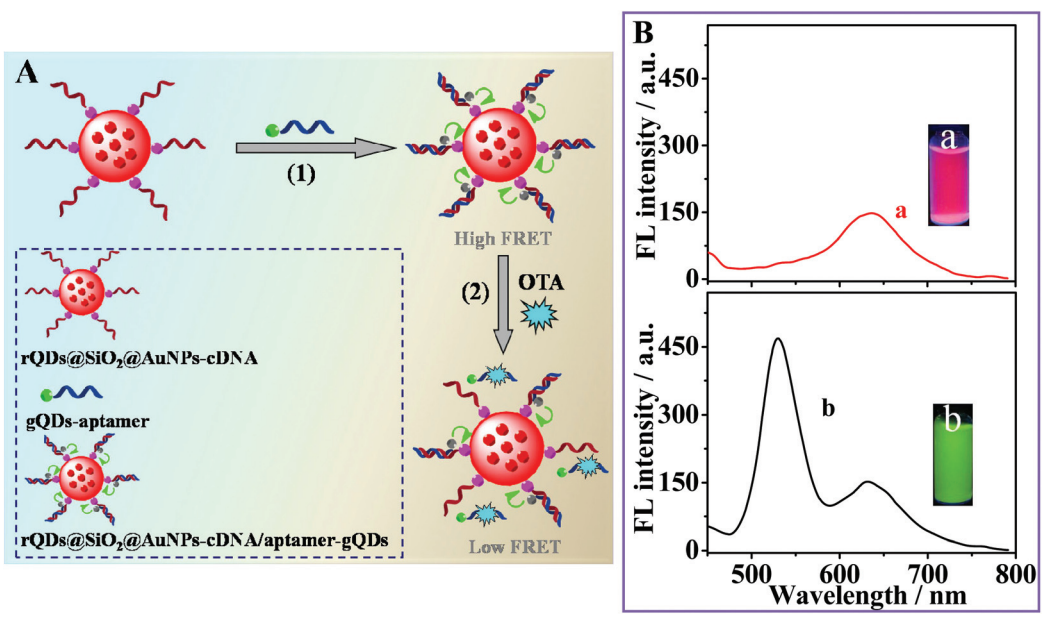

Fig. 3 (A) The working principle of the FRET-based ratiometric fluorescent aptasensor for OTA detection. (B) Fluorescence spectra and the corresponding photographs of the rQDs@SiO_2@AuNPs–cDNA/aptamer–gQDs bioconjugations in the absence (a) and presence (b) of 10 ng mL^{-1} of OTA.

(step 2 in Fig. 3A). In the absence of OTA, there was no target to bind with the aptamer and the FRET process was effective. Therefore, there were no gQDs dissociated from the bioconjugations and thus no fluorescence emission at 530 nm was monitored. In the presence of OTA, it could compete with the cDNA to bind with the aptamer to form the OTA–aptamer complex. This made preloaded gQDs dissociate from the bioconjugations and resulted in the interruption of the FRET process, leading to the fluorescence recovery of gQDs (curve b in Fig. 3B). Upon the "off–on" state of the green fluorescence and the background of the wrapped gQDs, a ratiometric fluorescent aptasensor was therefore realized for homogeneous OTA detection after only an incubation step. As the bioconjugations can be produced at a large scale in a single run, this strategy can be conveniently used for rapid detection of OTA without routine purification steps. More significantly, the changes in the intensity ratio of the dual emission wavelengths led to a remarkable fluorescence color change (photographs inset in Fig. 3B), thus facilitating the onsite naked eye detection of OTA in solution.

Optimization of experimental conditions

To generate a sensitive sensing system with rapid-response and low detection limit for OTA detection, experimental variables including temperature (Fig. 4A) and time (Fig. 4B) involved in the hybridization reaction for the preparation of the rQDs@SiO_2@AuNPs–cDNA/aptamer–gQDs bioconjugations were all optimized. The maximum fluorescence quenching efficiency of gQDs at 530 nm was observed at 37 °C and 120 min, through measuring the FL intensity of the mixture of the rQDs@SiO_2@AuNPs–cDNA and aptamer–gQDs after completing the hybridization reaction. Because the binding event between the aptamer and its target OTA is a time-dependent process, the effect of the incubation time for OTA binding was also investigated in detail (Fig. 4C). At the fixed concentration of OTA, the FL response obtained from the tested solution increased dramatically over time before 60 min, and then leveled off at time longer than 60 min. On this basis, 60 min was an appropriate incubation time for subsequent OTA detection.

Analytical performances of the aptasensor

Under the optimal conditions, the capability of the bioconjugations as an aptasensor for the OTA assay was investigated. Upon the introduction of increasing concentration of OTA into the rQDs@SiO_2@AuNPs–cDNA/aptamer–gQDs bioconjugations, the sensing system exhibited little emission change at 635 nm corresponding to the wrapped rQDs, while another fluorescence peak at 530 nm recovered gradually (Fig. 5A), which as expected, was a result of the dissociated gQDs due to the highly specific aptamer–OTA binding. The FL intensity at 530 nm ceased to increase beyond 10 ng mL^{-1} of OTA, indicating that the binding reaction was nearly saturated at this concentration. High concentrations of noninteracting donors and acceptors do not undergo FRET, hence, a typically purification step was not required for this aptasensor and a homogeneous OTA assay was thus successfully developed. The separation-free nature of the homogeneous assay could effectively shorten the aptasensing time and make the sensing procedure simplified.

Through analyzing the ratio of the dual-emission fluorescence intensity of the aptasensing system with the concentrations of OTA (Fig. 5B), we obtained a linear relationship (inset in Fig. 5B) between the value of $(I_g/I_r)/(I_g/I_r)_0$ and the logarithm of the concentration of OTA (c_{OTA}) over a broad range of 5 pg mL^{-1}–10 ng mL^{-1}. The linear equation could be represented by $(I_g/I_r)/(I_g/I_r)_0 = 10.261 + 3.6225\log(c_{OTA}/\text{ng mL}^{-1})$ with $R^2 = 0.9987$, where $(I_g/I_r)_0$ and (I_g/I_r) are the relative FL intensity of the bioconjugations in the absence and presence of OTA, respectively. The detection limit for OTA was calculated to be 1.67 pg mL^{-1} based on S/N = 3. Moreover, the bioconjugations appeared as a bright red fluorescence in the absence of OTA. The green fluorescence of the gQDs at 530 nm could be recovered gradually in the presence of the increasing amount of OTA. With the red fluorescence background of the wrapped rQDs, even a slight increase of the green emission could result in distinguishable color change from red to yellow-green in a broad OTA concentration range of 10 pg mL^{-1}–5 ng mL^{-1} (Inset in Fig. 5A). Therefore, the noticeable fluorescence color evolution obtained from the FRET-based ratiometric fluorescent aptasensor thereby provided a simple and rapid method for the visual detection of OTA by the naked

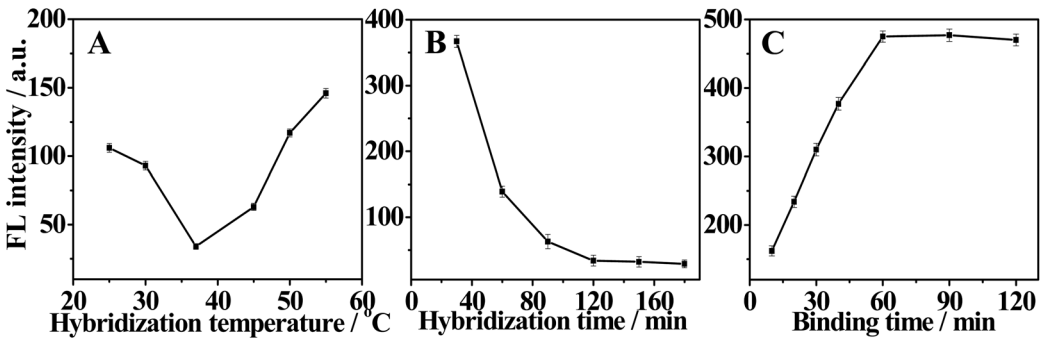

Fig. 4 The effects of hybridization temperature (A) and hybridization time (B) on the fluorescence intensity of the bioconjugations at 530 nm. (C) The effects of binding time on the recovered fluorescence intensity at 530 nm upon the exposure to 10 ng mL^{-1} of OTA.

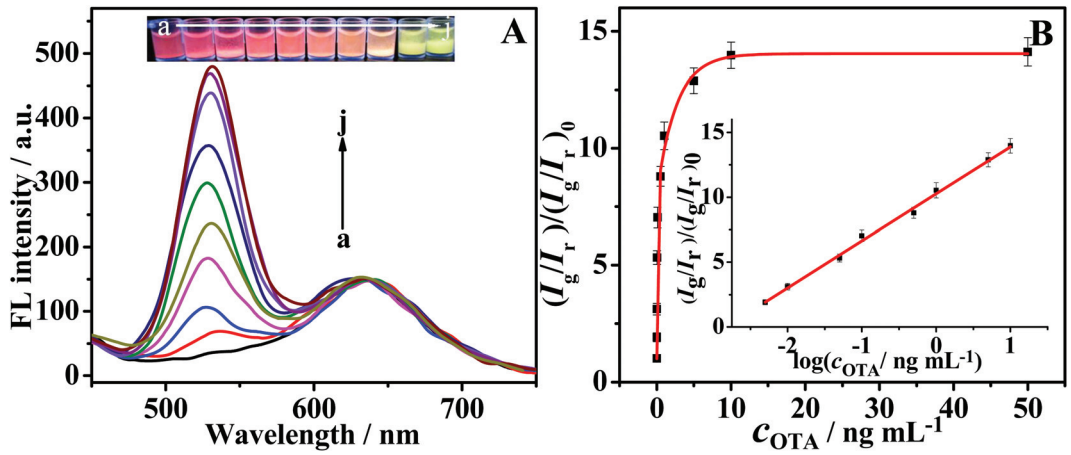

Fig. 5 (A) Fluorescence spectra and the corresponding photographs of rQDs@SiO_2@AuNPs–cDNA/aptamer–gQDs bioconjugations upon the exposure to different concentrations of OTA (from a to j: 0, 0.005, 0.01, 0.05, 0.1, 0.5, 1, 5, 10, and 50 ng mL^{-1}). (B) Plot of the $(I_g/I_r)/(I_g/I_r)_0$ *vs.* the concentration of OTA. Inset: the linear relationship for OTA detection.

eye or a home-used digital camera under a UV lamp. Characteristics of the present sensor along with others reported in the literature are all summarized in Table S1.† As can be seen, the present aptasensor possessed a broader linear range and lower detection limit, its sensitivity was higher than that of most other existed sensors for OTA.

The reproducibility of the aptasensor was also evaluated at the OTA concentration of 10 ng mL^{-1} (Fig. S4†), the relative standard deviation (RSD) for five independent measurements was 4.2%, indicating that the designed aptasensor for OTA detection was highly reproducible. The detection selectivity of the aptasensor was further studied by the comparison of the sensing results of OTA at the concentration of 10 ng mL^{-1} and 100 ng mL^{-1} of other related substances (FB1, AFB1 and OTB). As shown in Fig. S5,† the response signals to the potential interferents were negligible, attributing to the specific recognition force between the aptamer and OTA. This result indicated that this aptasensor possessed high specificity for OTA detection against other mycotoxins. In addition, the signal of the aptasensor showed no significant change in three weeks at the OTA concentration of 10 ng mL^{-1} (Fig. S6†), indicating that the aptasensor exhibited good long-term stability.

Detection of OTA in red wine samples

To demonstrate the application of the developed approach used for target analysis, the FRET-based aptasensor was performed to detect OTA by the standard addition method in the red wine samples subjected to a simple pre-treatment process according to the reported method.[50] Prior to determination, the filtered solution was adjusted to pH 7.4 with appropriate dilution (~10 fold) for later use. The results shown in Table 1 indicated that the average recoveries of spiked OTA ranged from 94.0% to 97.3% with a satisfying analytical precision (RSD ≤ 6.4%). All of the findings indicated the acceptable accuracy and validity of the proposed sensor as applied to OTA detection in real samples.

Table 1 Assay results for detection of different concentrations of OTA in red wine samples (n = 3)

Sample	Added (ng mL^{-1})	Detected (ng mL^{-1})	RSD (%)	Recovery (%)
1	0.05	0.047 ± 0.004	6.4	94.0
2	0.5	0.483 ± 0.013	5.8	96.6
3	5	4.865 ± 0.075	5.9	97.3

Conclusions

A novel ratiometric aptasensor has been developed for sensitive OTA detection by taking the advantages of FRET between gQDs and AuNPs attached on the rQD@SiO_2 spheres. Excellent fluorescence quenching was achieved between gQD-donor and AuNP-acceptor in the aptasensor construction, while the subsequent fluorescence recovery induced by OTA was obtained in the detection procedure. Based on the red background stably emitted by the wrapped rQDs, the aptasensor in response to increasing OTA displayed distinguishable color changes, which could be conveniently readout in solution even by the naked eye. The bioconjugations used as the aptasensor can be produced at a large scale and therefore this method can be conveniently used for *in situ*, rapid, or high-throughput OTA detection after only an incubation step. In comparison with the conventional ones, the proposed aptasensor is simple and time-saving because there is no separation of reactants and repeated washing steps involved. We believe that this novel aptasensing strategy provides not only a promising method for OTA detection but also a universal model for detecting

diverse targets in various fields by changing the corresponding aptamer.

Acknowledgements

This work was supported by the National Natural Science Foundation of China (no. 21405063, 21175061, and 21375050), the Natural Science Foundation of Jiangsu province (no. BK20130481), China Postdoctoral Science Foundation Funded Project (no. 2015T80517), Research Foundation of Jiangsu University (12JDG087), a project funded by the Priority Academic Program Development of Jiangsu Higher Education Institutions (no. PAPD-2014-37), and Key Laboratory of Modern Agriculture Equipment and Technology (no. NZ201109 and NZ201307).

Notes and references

1 F. Al-Taher, K. Banaszewski, J. Jackson, J. Zweigenbaum, D. Ryu and J. Cappozzo, *J. Agric. Food Chem.*, 2013, **61**, 2378–2384.
2 J. H. Park, J. Y. Byun, H. Mun, W. B. Shim, Y. B. Shin, T. Li and M. G. Kim, *Biosens. Bioelectron.*, 2014, **59**, 321–327.
3 A. Hayat, S. Andreescu and J. Marty, *Biosens. Bioelectron.*, 2013, **45**, 168–173.
4 S. J. Bellver, M. Fernández-Franzón, M. J. Ruiz and A. Juan-García, *J. Agric. Food Chem.*, 2014, **62**, 7643–7651.
5 R. Ghali, K. Hmaissia-Khlifa, C. Mezigh, C. Ghorbel, K. Maaroufi, S. Maschgoul and A. Hedilli, *Anal. Lett.*, 2008, **41**, 757–766.
6 N. W. Turner, S. Subrahmanyam and S. A. Piletsky, *Anal. Chim. Acta*, 2009, **632**, 168–180.
7 G. J. Soleas, J. Yan and D. M. Goldberg, *J. Agric. Food Chem.*, 2001, **49**, 2733–2740.
8 J. G. Pacheco, M. Castro, S. Machado, M. F. Barroso, H. P. A. Nouws and C. Delerue-Matos, *Sens. Actuators, B*, 2015, **215**, 107–112.
9 P. Novo, G. Moulas, D. M. F. Prazeres, V. Chu and J. P. Conde, *Sens. Actuators, B*, 2013, **176**, 232–240.
10 F. Y. Yu, M. M. Vdovenko, J. J. Wang and I. Y. Sakharov, *J. Agric. Food Chem.*, 2011, **59**, 809–813.
11 D. Flajs, A. M. Domijan, D. Ivić, B. Cvjetković and M. Peraica, *Food Control*, 2009, **20**, 590–592.
12 J. Zhang, X. Zhang, G. D. Yang, J. H. Chen and S. H. Wang, *Biosens. Bioelectron.*, 2013, **41**, 704–709.
13 N. Prabhakar, Z. Matharu and B. D. Malhotra, *Biosens. Bioelectron.*, 2011, **26**, 4006–4011.
14 J. Qian, L. Jiang, X. W. Yang, Y. T. Yan, H. P. Mao and K. Wang, *Analyst*, 2014, **139**, 5587–5593.
15 L. Rivas, C. C. Mayorga-Martínez, D. Quesada-González, A. Zamora-Gálvez, A. Escosura-Muñiz and A. Merkoçi, *Anal. Chem.*, 2015, **87**, 5167–5172.
16 J. A. Cruz-Aguado and G. Penner, *J. Agric. Food Chem.*, 2008, **56**, 10456–10461.
17 Q. Zhao, Q. Lv and H. L. Wang, *Anal. Chem.*, 2013, **86**, 1238–1245.
18 J. H. Chen, X. Zhang, S. X. Cai, D. Z. Wu, M. Chen, S. H. Wang and J. Zhang, *Biosens. Bioelectron.*, 2014, **57**, 226–231.
19 L. Rivas, C. C. Mayorga-Martinez, D. Quesada-González, A. Zamora-Gálvez, A. Escosura-Muñiz and A. Merkoçi, *Anal. Chem.*, 2015, **87**, 5167–5172.
20 P. Luo, Y. Liu, Y. Xia, H. J. Xu and G. M. Xie, *Biosens. Bioelectron.*, 2014, **54**, 217–221.
21 Z. P. Wang, N. Duan, X. Hun and S. J. Wu, *Anal. Bioanal. Chem.*, 2010, **398**, 2125–2132.
22 J. Lee, C. H. Jeon, S. J. Ahn and T. H. Ha, *Analyst*, 2014, **139**, 1622–1627.
23 Y. Wei, J. Zhang, X. Wang and Y. X. Duan, *Biosens. Bioelectron.*, 2015, **65**, 16–22.
24 C. Q. Wang, J. Qian, K. Wang, K. Wang, Q. Liu, X. Y. Dong, C. K. Wang and X. Y. Huang, *Biosens. Bioelectron.*, 2015, **68**, 783–790.
25 X. Y. Sun, B. Liu and Y. B. Xu, *Analyst*, 2012, **137**, 1125–1129.
26 C. M. Tyrakowski and P. T. Snee, *Anal. Chem.*, 2014, **86**, 2380–2386.
27 S. Goswami, A. K. Das, K. Aich, A. Manna, S. Maity, K. Khanra and N. Bhattacharyya, *Analyst*, 2013, **138**, 4593–4598.
28 S. Goswami, A. Manna, S. Paul, A. K. Maity, P. Saha, C. K. Quah and H. K. Fun, *RSC Adv.*, 2014, **4**, 34572–34576.
29 D. Schultz, S. M. Copp, N. Markesevic, K. Gardner, S. S. R. Oemrawsingh, D. Bouwmeester and E. Gwinn, *ACS Nano*, 2013, **7**, 9798–9807.
30 S. Goswami, S. Paul and A. Manna, *Tetrahedron Lett.*, 2014, **55**, 3946–3949.
31 D. Dinda, A. Gupta, B. K. Shaw, S. Sadhu and S. K. Saha, *ACS Appl. Mater. Interfaces*, 2014, **6**, 10722–10728.
32 W. Xu, Y. H. Xiong, W. H. Lai, Y. Xu, C. M. Li and M. Y. Xie, *Biosens. Bioelectron.*, 2014, **56**, 144–150.
33 D. Bu, H. S. Zhuang, G. X. Yang and X. X. Ping, *Sens. Actuators, B*, 2014, **195**, 540–548.
34 J. Qian, C. Q. Wang, X. H. Pan and S. Q. Liu, *Anal. Chim. Acta*, 2013, **763**, 43–49.
35 J. Y. Shi, C. Y. Chan, Y. Pang, W. W. Ye, F. Tian, J. Lyu, Y. Zhang and M. Yang, *Biosens. Bioelectron.*, 2015, **67**, 595–600.
36 Y. P. Shi, Y. Pan, H. Zhang, Z. M. Zhang, M. J. Li, C. Q. Yi and M. S. Yang, *Biosens. Bioelectron.*, 2014, **56**, 39–45.
37 K. Zhang, Q. S. Mei, G. J. Guan, B. H. Liu, S. H. Wang and Z. P. Zhang, *Anal. Chem.*, 2010, **82**, 9579–9586.
38 Z. J. Wang, J. Zhang, C. F. Zhu, S. X. Wu, D. Mandler, R. S. Marks and H. Zhang, *Nanoscale*, 2014, **6**, 3110–3115.
39 Z. X. Zhou, W. Wei, Y. J. Zhang and S. Q. Liu, *J. Mater. Chem. B*, 2013, **1**, 2851–2858.
40 W. W. Yu, L. H. Qu, W. Z. Guo and X. G. Peng, *Chem. Mater.*, 2003, **15**, 2854–2860.
41 W. Y. Liu, Y. Zhang, S. G. Ge, X. R. Song, J. D. Huang, M. Yan and J. H. Yu, *Anal. Chim. Acta*, 2013, **770**, 132–139.

42 T. T. Chen, Y. H. Hu, Y. Cen, X. Chu and Y. Lu, *J. Am. Chem. Soc.*, 2013, **135**, 11595–11602.
43 Y. L. He, J. N. Tian, J. N. Zhang, S. Chen, Y. X. Jiang, K. Hu, Y. C. Zhao and S. L. Zhao, *Biosens. Bioelectron.*, 2014, **55**, 285–288.
44 J. J. Zhang, F. F. Cheng, T. T. Zheng and J. J. Zhu, *Anal. Chem.*, 2010, **82**, 3547–3555.
45 R. J. Cui, C. Liu, J. M. Shen, D. Gao, J. J. Zhu and H. Y. Chen, *Adv. Funct. Mater.*, 2008, **18**, 2197–2204.
46 J. J. Zhang, T. T. Zheng, F. F. Cheng, J. R. Zhang and J. J. Zhu, *Anal. Chem.*, 2011, **83**, 7902–7909.
47 J. Wang, G. D. Liu, M. H. Engelhard and Y. H. Lin, *Anal. Chem.*, 2006, **78**, 6974–6979.
48 W. Park, M. J. Kim, Y. Choe, S. K. Kim and K. Woo, *J. Mater. Chem. B*, 2014, **2**, 1938–1944.
49 Y. Xiao, F. Shu, K. Y. Wong and Z. H. Liu, *Anal. Chem.*, 2013, **85**, 8493–8497.
50 W. Ma, H. H. Yin, L. G. Xu, Z. Xu, H. Kuang, L. B. Wang and C. L. Xu, *Biosens. Bioelectron.*, 2013, **42**, 545–549.